Journal of Drug Delivery Science and Technology 81 (2023) 104204

Contents lists available at ScienceDirect

Journal of Drug Delivery Science and Technology

journal homepage: www.elsevier.com/locate/jddst

Novel polyvinyl-alcohol microsphere for everolimus delivery for subependymal giant cell astrocytoma

Lynn Louis [a,1], Bor Shin Chee [a,1], Noreen Louis [d,1], Gabriel Goetten De Lima [c,1], Marion McAfee [b,1], Alan Murphy [a,1], Michael J.D. Nugent [a,1,*]

[a] Materials Research Institute, Technological University of the Shannon Athlone, Co. Westmeath, Ireland
[b] Centre for Mathematical Modelling and Intelligent Systems for Health and Environment (MISHE), Atlantic Technological University, Sligo, Ireland
[c] Federal University of Paraná, Programa de Pós-Graduação em Engenharia e Ciência dos Materiais – PIPE, Curitiba, Brazil
[d] John Radcliffe Hospital, Oxford University Hospitals, NHS Trust, Headley Way, Oxford, United Kingdom

ARTICLE INFO

Keywords:
Subependymal giant cell astrocytoma
Everolimus
Polyvinyl alcohol
Drug delivery system
Drug-release kinetics
Freeze-Thawing

ABSTRACT

Everolimus (EVR) has demonstrated efficacy in treating subependymal giant cell astrocytoma (SEGA) and other tuberous sclerosis (TSC) manifestations. Oral use of EVR is associated with low bioavailability and systemic toxicities culminating in treatment cessation in an appreciable patient population. To circumvent undesired effects, we developed a microsphere embedded formulation of EVR using polyvinyl alcohol (PVA) with an end-goal to achieve higher bioavailability and sustained delivery.

PVA-EVR microspheres were physically cross-linked using the freeze-thaw technique, and solvent-cast PVA-EVR films were developed as a control, without freezing and thawing cycles to ascertain the techniques significance. *In vitro* analyses and characterisation was performed to determine drug release and drug-polymer compatibility whereas *In silico* studies was done to analyse the non-crosslinked polymer and to evaluate qualitatively the interaction between EVR and PVA.

The PVA-EVR microspheres were found to have high encapsulation efficiency, resulting in sustained release of EVR when compared to solvent cast films. The molecular docking studies showed excellent compatibility of the drug-polymer combination, further confirmed by the characterisation studies performed using DSC, FTIR, SEM and XRD. The developed PVA-EVR microspheres in this study can serve as a highly effective drug-delivery system with better bioavailability in treating SEGA tumours.

1. Introduction

Subependymal Giant Cell Astrocytoma (SEGA) is a rare intraventricular low-grade benign tumour that causes obstructive hydrocephalus in patients with tuberous sclerosis complex (TSC). The aetiology of SEGA is due to an underlying rare genetic condition known as TSC and it appears in the subependymal nodules in the region of the foramen of Monro [1]. Therefore, treatment of SEGA tumours is considered more intricate due to the typical deep location of the lesion [2]. Standard therapy for symptomatic SEGA involves surgical resection to prevent obstructive hydrocephalus by relieving mass effect. Resection however is associated with perioperative morbidity and complications. For asymptomatic SEGA the current consensus recommends the use of the mammalian target of rapamycin (mTOR) inhibitor Everolimus [3].

Everolimus is an inhibitor of mTOR kinase and is a semi-synthetic 40-*O*-[2-hydroxyethyl] derivative of sirolimus. Everolimus acts as a proliferation signal inhibitor and an active immuno-suppressor. Previously, Franz et al. [4] reported the regression of SEGA following treatment with rapamycin. The mTOR inhibitor is blocked by rapamycin by binding to the FKBP12 protein, causing a cell cycle arrest at the G1/S phase, which ultimately prevents T-cell proliferation and stimulation [5,6]. In addition, EVR was shown to block the specific molecular defect that caused TSC by inhibiting the mTOR complex 1 [7]. Although orally administered EVR has been proven to clinically improve the treatment of SEGA, however the severe side effects related to EVR have led to considerable treatment interruption or dose reduction [8]. Given its very hydrophobic nature, EVR has shown significant pharmacokinetic limitations, which include the limited absorption of EVR due to its poor

* Corresponding author.
E-mail address: mnugent@ait.ie (M.J.D. Nugent).
[1] These authors contributed equally to this work.

https://doi.org/10.1016/j.jddst.2023.104204
Received 27 September 2022; Accepted 23 January 2023
Available online 2 February 2023

water solubility, extensive metabolism by the liver's cytochrome P450 enzyme (CYP3A4, CYP3A5, and CYP2C8), and exposure to an early metabolic response by the liver and p-glycoprotein (p-gp) mediated efflux [4,7]. Other reported side effects of EVR include immunosuppression (infections, mouth sores) and hypercholesterolemia, which warrants regular drug monitoring [9–12].

Furthermore, it is crucial to achieve optimal exposure levels when using EVR due to its narrow therapeutic index [12,13]. Cessation of treatment with EVR may result in tumour re-growth [13]. Therefore, microspheres have been considered the appropriate drug delivery carrier, particularly to prolong the effective use of EVR, due to their excellent suspension stability and unique properties. Microspheres are also easily employed as implantable carriers in brain tumour therapy via stereotactic surgery (the use of three-dimensional (3D) coordinates) and are potent carriers of chemotherapeutic drugs, as reported by Menei [14]. Interestingly, newly developed microspheres, such as 1,3-bis (2-Chloroethyl)-1-nitrosourea (Gliadel), have been approved by the United States Food and Drug Administration (US FDA) for the treatment of glioblastoma. Hence, the potential use of microspheres as a drug delivery device has attracted the attention of the research community to minimise long-term invasive surgery and to help prolong drug release. Various polymer drug delivery systems have been studied in the past few years, such as polyethene glycol-polylactic acid (PELA), chitosan, and sodium alginate. Nevertheless, the downside of these carriers includes the significant amount of residual organic solvent, high toxicity, and poor stability [15]. Alternatively, Polyvinyl Alcohol (PVA) has demonstrated promising advantages in the preparation and application of microspheres [15]. Based on recent *in vitro* and *in vivo* studies, the semi-crystalline polymer exhibited exceptional biocompatibility, hydrophilicity, biodegradability, and non-toxic properties [15–17]. A smaller microsphere possesses a larger surface area to volume ratio, which enhances the encapsulation and drug release from the microsphere via diffusion and surface erosion with the ability to cross the blood-brain barrier [14,15].

In this study, we investigate the development of a novel polymer-based drug delivery system by encapsulating EVR in a PVA-based microsphere to achieve a sustained local delivery of EVR to treat SEGA. The physicochemical properties of the combined EVR-loaded microspheres using PVA (PVA-EVR) were characterised, followed by determining the performance of the PVA-EVR microsphere, which includes the encapsulation efficiency, *in vitro* EVR release kinetic model studies, swelling index and weight loss studies. For comparison purposes, solvent-cast PVA-EVR films were prepared with similar molecular weight, grade, and drug concentration without undergoing freeze-thaw cycles to further demonstrate the effects of crosslinking on the microspheres. To the best of the author's knowledge, the entrapment of EVR in PVA has not been attempted before in the treatment of SEGA-associated TSC, thus, highlighting the novelty of this study.

2. Materials and methods

2.1. Materials

This study employed several PVA derivatives with varying average molecular weight (Mw), and different Mowiol grades of PVA (Mw = 13,000–23,000 g/mol, 87–89%), PVA grade Mowiol 18–88 (Mw = 130,000 g/mol, 88%), PVA grade Mowiol 28–99 (Mw = 145,000 g/mol, 99%), and PVA grade Mowiol 56–98 (Mw = 195,000 g/mol, 99%). All PVA derivatives were purchased from Sigma Aldrich Chemistry Co. (St. Louis, MO, USA), while EVR (>99% purity) was purchased from LC Laboratories (Woburn, MA, USA).

2.2. Optimisation of PVA and EVR concentration

Preliminary studies were performed to examine the formation of microspheres. To obtain the microspheres, a series of experiments with different PVA concentrations (1–15 wt %) and EVR contents (0.5 and 1 wt %) per weight in volume was tested with different molecular weights and Mowiol grades listed in (Table 1). The optimisation of PVA and EVR concentration was then carried out based on the full factorial design generated by Minitab Statistics software Version 17 with three varying parameters comprising the PVA grade, PVA concentration, and EVR concentration. The criteria applied for the final selection of the PVA grade and concentration was based on the ability of the spheres to retain its shape during the F/T cycles and freeze-drying process.

2.3. Preparation of freeze-thaw PVA-EVR microspheres

Prior to the microsphere production, 0.5 g of PVA was dissolved in 9 mL in a bottle of distilled water at 100 ± 5 °C on a hot plate under a magnetic stirring rate of 500 ± 10 rpm for 2 h. A clear uniform solution should be visible after the polymer solution was completely dissolved. The polymer solution was then left to cool at Room Temperature (RT) for 1 h. The EVR stock solution was prepared separately by dissolving 100 mg of EVR in 1 mL of pure ethanol (EtOH) to achieve a final concentration of 1% w/v. Next, the EVR solution was added drop-by-drop into the cooled polymer solution using a micropipette with continuous stirring at 500 rpm to obtain a homogenous solution. The PVA-EVR solution was then left to stir for 1 h at RT.

The microspheres were developed by dispensing the 10 mL of PVA-EVR solution using a 100 μL micropipette into a plastic vial containing 2 mL of pre-cooled ethanol immersed in a canister containing 100 mL of liquid nitrogen (−196 °C), where the droplets would instantly solidify. Then, the freeze-thawing technique was performed. For the initial freezing step, the frozen microspheres were immediately placed in a −80 °C freezer for 30 min and subsequently placed in a −20 °C refrigerator for 30 min. This step was repeated three times and was labelled as the 3 freezing (3F) cycle. After completing the 3F cycles, the frozen microspheres were thawed at RT for 30 min until the microspheres were defrosted and re-frozen at −80 °C for 30 min. This step was repeated 3 times and was labelled as the 3 thawing (3T) cycle.

Although the microspheres were initially subjected to 3F cycles and 3T cycles (3F/3T), the microspheres could not retain their shape during the thawing process (see Supplementary Material Fig. S1). Subsequently, the number of freeze-thawing cycles was increased to 6 freezing cycles and 3 thawing cycles (6F/3T) (Table 2), which successfully achieved a well-defined shape. The number of freeze-thaw cycles corresponds to the maximum limit of three freeze-thaw cycles for EVR, as stated in the manufacturer's Certificate of Analysis (COA).

A Heto PowerDry® LL1500 Freeze Dryer was used to evaporate the residual ethanol from the microspheres post-freezing-thawing cycles. Subsequently, the freeze-dried sample was covered in aluminum foil to evaporate ethanol completely and left overnight. Finally, the sample was stored in a −20 °C refrigerator before proceeding with the dissolution analysis. The overall process of this study follows that of a recently published synthesis of PVA microspheres using a combination of different drugs [15].

Table 1
The varying concentrations of PVA in conjunction with the varying EVR concentration prepared at each molecular weight and Mowiol grade.

Variables	Conditions
Concentration of PVA (%w/v) tested	1 2 3 4 5 10 15
Concentration of EVR (%w/v) tested	0.5% and 1% for each PVA Concentration
Molecular Weight (g/mol)/% Hydrolysis for each PVA concentration tested	13,000–23,000/18–88 130,000/18–88 145,000/28–99 195,000/56-98

Table 2
The varying freeze-thaw cycles used in this study.

	Method 1 (3F/3T)	Method 2 (6F/3T)
Number of freezing cycle (F)	3	6
Temperature 1 (°C)	−80	−80
Temperature 2 (°C)	−20	−20
Number of thawing cycle (T)	3	3
Thawing temperature (°C)	RT	RT
Re-freeze temperature (°C)	−80	−80

*Note: Length of freezing cycle = 30 min; Length of thawing time = 30 min.

2.4. Development of solvent-cast PVA-EVR film

To determine the impact of freeze-thawing on the crosslinking between PVA and EVR, the solvent-cast PVA-EVR film was prepared following the same procedures as the PVA-EVR microsphere development in Section 2.3 except without the freeze-thaw cycle process. Instead of transferring into plastic vials for the freeze-thaw process, approximately 3 mL of the developed PVA-EVR solution was cast onto a clean plastic Petri dish and stored at RT under dark conditions for two days to allow the solvent to completely dry before conducting the *in vitro* drug release test.

2.5. Physicochemical characterisation of PVA-EVR microspheres

The physical, chemical, and thermal properties of the developed microspheres and films were evaluated using various methods, as presented in the following section.

2.5.1. Differential scanning calorimetry (DSC)

A Pyris PerkinElmer DSC instrument was used to determine the complexation of the PVA-EVR formulation based on the resultant shifts in the endothermic peaks relative to the pure PVA and EVR [5]. Approximately 3–5 mg of sample was weighed using DSC Aluminum pans. The sample was then heated at 10 °C/min over a range of 30–270 °C under nitrogen gas flow. Conversely, the sample was heated at 10 °C/min over a range of -60 -110 °C under nitrogen gas flow to obtain the glass transition temperature (Tg) value of pure EVR. The Pyris PerkinElmer software (Waltham, MA, USA) was used to analyse the collected data. The degree of crystallinity (Xc) of the hydrogel samples from the endothermic area was calculated based on the following equation [17]:

$$Xc = \Delta Hf / \Delta Hf_o \qquad \text{Equation 1}$$

where ΔHf represents the measured enthalpy of fusion of the PVA microsphere and ΔHf_o is the thermodynamic enthalpy of fusion for 100% crystalline PVA (ΔHfo = 150 J/g) [18,19].

2.5.2. Thermogravimetric analysis (TGA)

The decomposition temperature and percentage weight loss of EVR were determined using a PerkinElmer Pyris 1 TGA under a nitrogen-air flow at 40–60 mL/min. Approximately 3–5 mg of EVR sample was placed in an aluminium pan and heated from 25 °C to 600 °C at a rate of 10 °C/min.

2.5.3. Scanning electron microscope (SEM)

The surface morphology of the prepared PVA-EVR microspheres was examined using a TESCAN SEM (Brno, Czech Republic). Prior to the analysis, the sample was sliced to view the cross-sectional region. Subsequently, the sample was deposited on a silver stub under vacuum conditions and sputter-coated with gold in a Baltec SCD 005 sputter coater for 110 s at 0.1 mbar vacuum to yield a uniform coating of ca. 110 nm on the stub. The surface morphology was then viewed using the SEM instrument.

2.5.4. Fourier transformed infrared spectroscopy (FTIR)

FTIR analysis was carried out to determine and compare the functional groups of the PVA-EVR microspheres with pure EVR and PVA microspheres. A PerkinElmer Spectrum One FTIR Spectrometer equipped with the FTIR spectrum one software was employed to analyse the samples. Once freeze-dried, the sample was placed on a diamond crystal sample holder. The data was collected in the spectral range of 4000–400 cm^{-1} at 4 scans per sample cycle and fixed universal compression force of 78 N. Subsequent analysis was performed using a PerkinElmer Speckwin32 spectroscopy software [20].

2.6. In vitro EVR release kinetic model studies

The *in vitro* EVR release kinetics of the PVA-EVR formulation were evaluated using the USP (United States Pharmacopeia) Apparatus 1 method. Approximately 0.2–0.4 g of the dried microspheres was placed into a rotating basket containing 500 mL of phosphate buffer and stirred at 100 rpm for a total of 12.5 days at 37 ± 1 °C and a pH of 7.4. A total of 2 mL of aliquot was collected at different time intervals of 10, 20, 30, 40, 50, and 60 min, followed by each hour for the first 8 h and then every 24 h (at the same time point) for the next 12.5 days until no further release of EVR was observed. Each collected sample was then replaced with 2 mL of phosphate buffer. The test was done in triplicate. The EVR concentration in the collected samples was analysed immediately using a UV-1280 Shimadzu Ultraviolet–visible (UV–vis) spectrophotometer at 278 nm. The absorbance of the blank PVA microspheres was measured and subtracted from the sample (PVA-EVR microspheres) absorbance to remove any interference from the residual PVA microspheres used. The obtained value was inserted into the equation from the standard EVR calibration curve (y = 11.274x - 0.0673) (Supplementary Fig. 8) and multiplied by 500 mL to obtain the experimental value of the EVR released in the vessels. The results were then input into the DDSolver software to obtain the cumulative drug release percentage.

Additionally, various model-dependent approaches were used, including the first-order, zero-order, Higuchi, Korsmeyer-Peppas, and the Hixson-Crowell model, to determine the release profile of EVR from the microspheres. The first-order model describes the concentration-dependent drug release, while the zero-order model defines a drug release that is not influenced by the concentration and the dissolved substance. In addition, the Higuchi model implies that the drug release occurs via diffusion according to Fick's law. Moreover, the Korsmeyer-Peppas model assumes that the drug release from polymeric material is governed by the value of the release exponent (n). A Fickian diffusion mechanism is indicated by $n = 0.45$, while a non-Fickian diffusion (also known as a case II relaxation) is represented as $n = 0.89$. Besides, the $n > 0.89$ describes a super case II transporter, while $0.45 < n < 0.89$ indicates an anomalous diffusion or a non-Fickian diffusion [21]. Finally, the Hixson-Crowell model assumes that the drug release mechanism is controlled by the dissolution and the surface area changes as well as the particle or tablet diameter [22]. The fitting level of the data to each model was evaluated using the determination coefficient (R^2) [17]. The model which gave the highest coefficient of determination (R^2) was the most suitable kinetic model for describing the release of EVR from the microspheres.

2.7. Calibration curve

A standard EVR stock solution at 0.2% (w/v) concentration was prepared by dissolving 2 mg of EVR in 1 mL of pure ethanol. Next, the EVR stock solution was diluted with phosphate buffer to obtain a concentration range from 0.007812 mg/mL to 0.07 mg/mL in separate Eppendorf tubes. Each diluted solution was then scanned using a UV–vis spectrophotometer at a range of 190–400 nm with phosphate buffer at pH 7.4 as a blank. The wavelength corresponding to maximum absorbance (λ max) was found to be 278 nm. Thus, the absorbance of each diluted solution was measured at 278 nm. The calibration curve was

obtained by plotting the absorbance value versus concentration data (Supplementary Fig. S8).

2.8. Encapsulation efficiency (EE)

The amount of Everolimus encapsulated in the microspheres were determined using a UV–Vis spectrophotometer (Shimadzu UV-2450). An accurately weighed 100 mg of microspheres were crushed and stirred in 10 mL of PBS buffer (pH 7.4) to disrupt the polymeric coat and centrifuged. The supernatant was then extracted in ethanol. The solution was stirred overnight [23]. The solution was then filtered through a 0.20 non-pyrogenic sterile filter after appropriate dilution with phosphate buffer and the drug content was determined at 278 nm which corresponds to the UV active functional group of EVR [19]. Note that the absorbance of the EVR was not affected by the polymer at the specified wavelength (Supplementary Fig. S6). The EE of the drug-loaded spheres was determined by calculating the following formula [23,24]:

Theoretical drug loading (%) = (Weight of drug added(g) / Weight of microspheres and drug added) x 100 (g) Equation 2

Actual drug loading (%) = (Experimental drug loading(g) / Theoretical drug loading(g)) x 100% Equation 3

Entrapment Efficiency (EE%) = (Actual amount of drug loaded in microspheres(g) / Theoretical amount of drug loaded in microspheres (g)) x 100% Equation 4

2.9. Swelling index and weight loss studies

The swelling index of the microsphere was determined by immersing the freeze-dried PVA-EVR microsphere in a vial containing PBS buffer at pH 7.4 at RT at intervals of 10, 20, 30, 60, 120,240,320, 1440 and 2880 min. The weight of the microsphere was first measured using an analytical balance at pre-determined time intervals until a constant weight was obtained. Subsequently, the excess surface-adhered liquid drops were removed by blotting the sample with filter paper and the microspheres were weighed again. The microspheres were re-immersed in the buffer again and left over 48 h. The percentage water content was calculated based on the following equation, where W_t is the weight of the swollen microsphere at pre-determined intervals, W_s is the swelling equilibrium state of the swelled microsphere, and W_d is the weight of the dried microsphere:

$$\text{Water content } (\%) = (W_t - W_d \,/\, W_S - W_d) \times 100\% \quad \text{Equation 5}$$

The degree of swelling was also calculated, where W_t represents the weight of the microsphere in the swollen state at a specific time and W_o is the weight of the microsphere in the dried state (Equation (6)). Finally, the percentage weight loss was calculated, as shown in Equation (7) [25]:

$$\text{Swelling ratio} = (W_t – W_o \,/\, W_0) \quad \text{Equation 6}$$

Weight loss (%) = (Original weight(g) – Re-dry weight(g)) / Original weight (g) × 100% Equation 7

2.10. Pre-liminary processing of molecules prior to molecular docking

To conform the structures for docking procedure, they were first set for a structure minimization. Everolimus 3D structure was obtained from chemspider (CSID:21106307), checked against protonation states using MarvinSketch (Chemaxon, Budapest, Hungary). Minimization of energy was performed using Avogadro software with GAFF force field [26] and followed by optimisation using a semi-empirical PM7 method within MOPAC2016 software [27], converting the files using open babel [28].

For the polymer structure, the polymer-builder from CHARMM-GUI [29] was used with 3500 monomeric units of PVA containing a syndiotatic structure with CH_3 end groups. The system was exposed to a dilute solution system in a cubic box type (XYZ:70 Å) with a single polymeric chain containing a polymer solvent ratio of 98% v/v. These settings were the maximum that could be achieved without an overlap in computation time from CHARMM-GUI allowed by the server cloud. To equilibrate the system, Kuhn Bead groups were calculated forming clusters of monomers within the polymeric chain, using the coarse-grained model. The interaction matrix and solubility parameter, consisted of a set of data that ranged from 0 to 2.14 $MPa^{1/2}$ calculated by the energy of dispersion, polar and hydrogen bonding forces. Equilibration of the system was performed with Openmm based on the hypothesis that the solvent acts as a liquid of LJ particles from same size and mass of the monomeric clusters. Interaction between beds is controlled by varying the cross-interaction parameter lambda (λ), set as ideal interaction (λ = zero) for this system. Temperature of the simulation was set to 300 K with a simulation time of 1000 ns?

The protein structure was obtained from 5FLC protein data bank. The protein was modified with DeepView/Swiss-PdbViewer for missing chains [30]. Chains were generated between atoms closer than 2 Å. For further analysis, only the chain F- related to serine/threonine-protein kinase mTOR, chain G - related to FKBP (intracellular receptor, FK506-binding protein) and the ligand were used.

2.11. Docking and re-docking procedure

For re-docking of protein and ligand, the autodocktools was used [31]. Water molecules was removed, and hydrogens atoms were added, merging non-polar ones, and addition of partial charges to protein (Kollman charges), containing FKBP and ligand (gasteiger charges), whereas the active bonds were fixed as non-rotatable. Grid box size was calculated using the coordinates of built-in ligand and a box spacing of 0.375 Å was used. The ligand parameters, genetic algorithm, docking run and parameters were set as standard values with a Lamarckian search algorithm output. For docking procedure of Everolimus, two docking configurations were performed, the first step involved only the protein and the drug, and the second step involved the protein + FKBP and the drug with flexible rotatable chains of the ligand.

For docking of PVA chains with EVR, autodock Vina [32] was used. Same procedure was performed as in AutoDock Tools, with the ligand being as flexible rotatable chains with spacing of 1 Å for gridbox with a blind dock using the whole polymer structure as the gridbox. Albeit with no redocking, as only a qualitative analysis was inferred. Parameters for AutoDock Vina were 4 CPU usages, and exhaustiveness of 100 and 10 number of poses.

2.12. Statistical analysis

The GraphPad Prism Version 9 software (La Jolla, CA, USA) was used to carry out the statistical analysis, which include the one-way Analysis of Variance (ANOVA) test, followed by the Tukey post-hoc test and a nomality test. The results were considered significant when $p < 0.05$.

3. Results and discussion

3.1. Optimisation of PVA and EVR concentration

Based on the optimisation results, it was found that the PVA Mowiol grade 56–98 with a concentration per weight in volume and Mw of 5% w/v and 195,000 g/mol, respectively, and 1% w/v of EVR achieved the optimum strength and viscosity to maintain the microsphere shape post-freeze drying. In contrast, the polymer solution at a concentration of 10%w/v and 15% w/v PVA 195,000 g/mol were too viscous to produce

microspheres using the droplet technique (100 μL micropipette) compared to the 5%w/v. This was due to the increasing particle size of microspheres as the solution concentration increased [33]. On the other hand, the PVA 195,000 g/mol with a concentration per weight in volume of 1w/v–4w/v% exhibited poor viscosity. Therefore, the microspheres were unable to retain their shape during the thawing cycle (Supplementary Material Fig. 1).

A similar phenomenon was observed for PVA Mw (13,000–23,000 g/mol, 130,000 g/mol and 145,000 g/mol) at polymer solution concentrations per weight in volume of 1, 2, 3, 4, 5, 10, and 15%w/v, respectively, where the microspheres could not maintain their shape due to the lack of viscosity. It was also observed that the concentration of EVR decreased the viscosity of PVA but at least 1% w/v of EVR was required to form stable microspheres. Therefore, it was established that 5%w/v of PVA 195,000 g/mol and high % hydrolysis together with the established 1% w/v EVR was the best option to achieve stable PVA-EVR microspheres.

3.2. Preparation of microspheres

The sessile droplet technique produced white and spherical microspheres, as shown in Fig. 1. When the EVR solution was added to the polymer mixture under constant stirring at 500 ± 10 rpm, the solution turned slightly cloudy permanently. Given that the added ethanol (1 mL) and deionised water were completely evaporated during the freeze-drying process, the prepared microspheres were safe to use without any trace of toxic chemicals. When the number of freezing cycles was increased, the microspheres were able to retain their shape, indicating that the crystal structure was strengthened. Thus, the 6F/3T cycles enhanced the physical crosslinking of the PVA-EVR microspheres, which maintained the spherical shape of the microsphere and prevented the initial burst release of the drug [16].

3.3. Physicochemical characterisation of PVA-EVR microspheres

3.3.1. DSC and TGA evaluation

The DSC analysis showed that the α-relaxation of PVA microspheres after 6F/3T and 3F/3T cycles were 51 °C and 50 °C, respectively. However, a decrease in the α-relaxation was observed at 40 °C for the freeze-thawed PVA-EVR microspheres. Chee et al. [17] demonstrated that the typical α-relaxation peak of PVA was 40–64 °C [17]. Additionally, a broad peak at 145 °C and 140 °C was observed in PVA microsphere samples with 6F cycles and 3F cycles with thawing, which represents the evaporation of residual water. The peak broadening was due to the β-relaxation as a result of the relaxation of the domains in the PVA crystalline regions.

Meanwhile, the manufacturer's COA stated that the melting point (Tm) of EVR was around 97–101 °C [8]. Based on the DSC analysis, pure EVR recorded a peak at 88.93 °C, which corresponded to the value reported in the literature [5] (Fig. 2), confirming the purity of the sample and its crystallinity.

The peak at 222 °C represents the Tm of the PVA crystalline domains, and the PVA-EVR microsphere showed a decreased endothermic peak from approximately 222 °C–220 °C. The decrease in Tm was due to crystallinity reduction caused by the presence of EVR in the microspheres. A similar effect was observed in recent studies conducted using caffeine and PVA, whereby an increase in caffeine altered the crystallisation of PVA and decreased the Tm and degree of crystallinity of caffeine-PVA [17]. As observed in the DSC thermogram, the degradation of EVR corresponded to a temperature shift from 192 °C to 181 °C. The result suggests that EVR was converted to an amorphous state when dissolved in the PVA solution, which then interferes with the organisation of the polymeric chain of PVA and consequently lowers the degree of crystallinity with its semicrystalline Tm of the hydrogel [34,35]. However, it is important to state that the degradation temperature of EVR is increased, because no thermal transition is seen when bonded with PVA at the region of 180–200 °C related to its intra- and inter-molecular bonds of PVA chains.

Furthermore, the degree of crystallinity was calculated by determining the area under the melting peak. As expected, the degree of crystallinity increased from 18.6% to 60.5% as the number of freezing cycles increased from 3F cycles to 6F cycles, respectively. It was assumed that the formation of smaller ice crystals increased as the degree of crystallinity increased. However, the addition of EVR to the PVA microspheres post-6F cycles reduced the degree of crystallinity to 35.9% due to the homogenous mixture of EVR in the PVA microsphere in the now amorphous state.

3.3.2. FTIR analysis

Fig. 3 illustrates the ATR-FTIR overlayed spectra of pure EVR, placebo sample (PVA microspheres), and PVA-EVR microspheres. The representative peaks for pure EVR were detected at 3402 cm^{-1} (OH), 2931 cm^{-1} (CH_3), 1643 cm^{-1} (C═O), 1451 cm^{-1} (*C*–H) bending for CH_2, and 990 cm^{-1} (*C*–H) [36–39]. Comparatively, the spectrum of the PVA-EVR microspheres presented an overlapping spectrum of EVR and the corresponding PVA spectrum with most of the characteristic peaks maintained except for the disappearing peak at 990 cm^{-1}. The presence of OH groups at 3279 cm^{-1} in the PVA-EVR microspheres was likely due to the increase in hydrogen bonds as a result of crosslinking. In addition, the peak observed at 1643 cm^{-1} in pure EVR corresponds to the amide (C═O) group but was replaced by another peak at 1658 cm^{-1} in the PVA-EVR microspheres. These results revealed that hydrogen bonds were formed between the carbonyl of PVA and the hydroxyl of EVR as well as between the carbonyl of EVR and the hydroxyl of PVA.

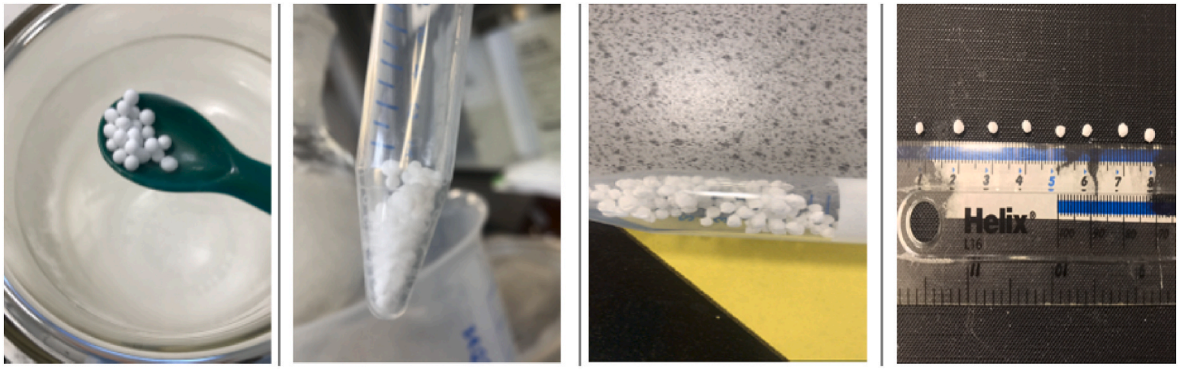

Fig. 1. a) Frozen microspheres before the freeze-drying technique; b) Microspheres during the freeze-drying process; c) Microspheres post-freeze-drying; (d) Measurement of microspheres-post freeze-drying.

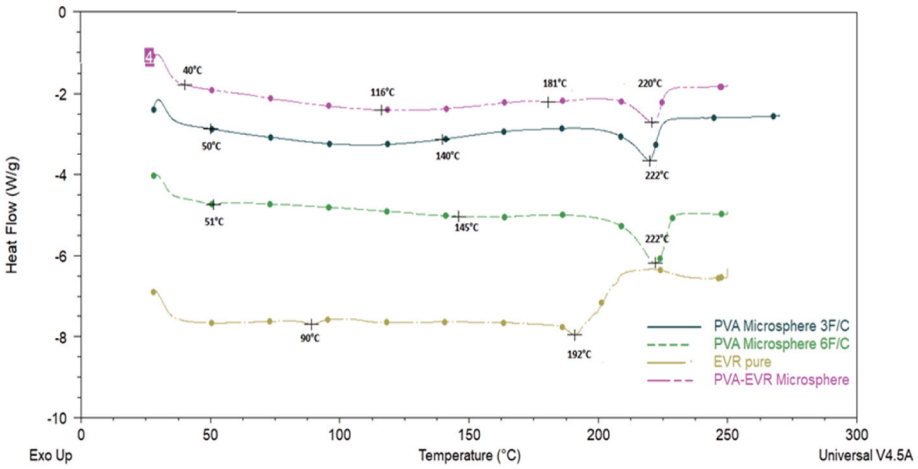

Fig. 2. The thermal transitions from the DSC analysis for a) EVR Pure, b) PVA-EVR microsphere, c) PVA microsphere 3F/C, and d) PVA Microsphere 6F/C.

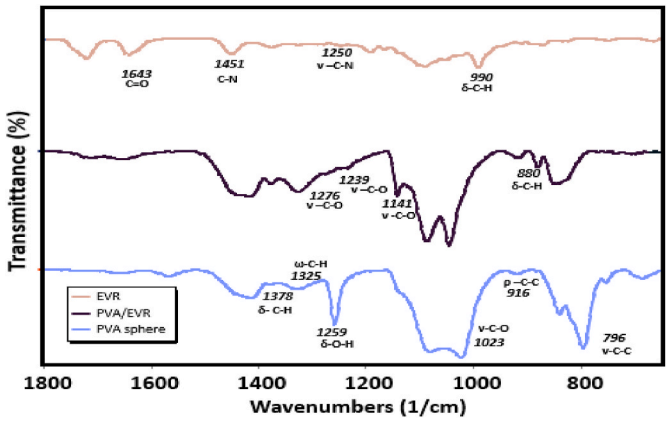

Fig. 3. FTIR analysis of pure EVR, PVA microsphere, and PVA-EVR microspheres.
Note: ν = stretching, δ = bending, ρ = rocking, ω = wagging.

As observed in Fig. 3, the OH bending peak observed at 1259 cm^{-1} in pure PVA disappeared, which was also detected by Shin et al. [40] and Tangtuam et al. [41] However, the peak was detected as a shoulder peak at 1276 cm^{-1} in the PVA-EVR microspheres, which showed a hypochromic blue shift among the free and entrapped EVR. Additionally, the peak representing the *C*–O aromatic ester in pure EVR at 1250 cm^{-1} shifted to 1239 cm^{-1} in the PVA-EVR microsphere, which denotes a *C*–O stretch (an ether) probably due to the interaction between the OH bending at 1259 cm^{-1} in PVA microspheres and the *C*–O aromatic ester. According to literature, the degree of crystallinity can be measured by intensity of the band at 1141 cm^{-1} for pure PVA which is influenced by the crystalline portion of the polymer chains. Therefore, this band is related to the symmetrical stretching of the *C*–C bond or the stretching of the *C*–O of a part of the chain where intramolecular hydrogen bonds are formed between two OH groups [42] and neighbours that are on the same side of the plane of the carbon chain. As expected, the crystalline portion is dependent on the number of OH groups in the PVA and, therefore, on the degree of hydrolysis, for the formation of hydrogen bonds. However, seen that EVR presents three possible OH interactions with PVA, this band represents the interaction between the drug with PVA seen that the crystallinity decreased by the thermal analysis [35, 43].

It is worth mentioning that a new peak at 881 cm^{-1} in the PVA-EVR microspheres represents the *C*–H bending, which can be explained by the merging of two peaks at 891 cm^{-1} and 871 cm^{-1} in the pure EVR. The formation of this new peak suggests the improved amorphous state of EVR, followed by the interaction between PVA and EVR since this peak was not observed in both PVA microspheres and pure EVR. This was also confirmed by the decrease in Tm from the DSC analysis.

3.3.2.1. Molecular docking. *In silico* studies were carried out to analyse the polymer, non-crosslinked and evaluated qualitatively interaction between EVR and the polymer (Figs. 4–5.). Overall, two hydrogen bonds were perceived in a single monomer of the drug with the PVA chain, confirming the overall good interaction between PVA and EVR due to the hydrogen bond group between OH groups.

Interactions occurred (Fig. 5.) in the OH group of the upmost, and freer, OH site of its molecule and within a region of concentrated Oxygen double bonds that are unstable, confirmed by their homo orbitals. Thus, confirming that self-binding of PVA may no longer be feasible and interaction with the drug is energetically more favourable presenting a binding affinity of −9.3 kcal/mol, confirming the decrease in chains ordering, related to crystallinity and this is confirmed by the FTIR results.

3.3.3. SEM observation

The morphology of the PVA-EVR microspheres and PVA microspheres was examined using SEM. Fig. 6A shows the spherical shape of the pure EVR powder. Comparatively, a smoother surface was observed for the PVA-EVR microsphere (Fig. 6B) compared to the PVA microsphere (Fig. 6I), which could be attributed to the use of ethanol during the formation of the PVA-EVR microsphere [38] as well as the varying liquid-liquid phase separation processes of PVA-EVR solution in ethanol. However, the addition of EVR decreased the pore size of the PVA-EVR compared to PVA microspheres. On the contrary, a fibrous-like structure was observed on the surface of the PVA microsphere [44], as shown in Fig. 6H.

The overall shape of the microsphere was influenced by the Mw (195,000 g/mol) of the PVA, the number of freezing and thawing cycles performed, and the type of solvent used to dispense the PVA-EVR solution, which is ethanol for this study. The result also emphasised the importance of selecting the appropriate solvent to obtain regular polymer microspheres.

Moreover, Fig. 6F shows that the microstructure of PVA-EVR microspheres fabricated through the freezing/thawing cycle process formed a 3D network supported by PVA walls [17]. The internal structure was investigated by analysing the cross-section of PVA-EVR microspheres, as observed in Fig. 6D and 6E. The interior section showed the unidirectional alignment of the PVA-EVR microsphere and a similar porous structure to the surface of the microsphere. A comparable phenomenon was also reported for PVA and caffeine in a previous study [17]. In short, the obtained porous structures were essential to construct

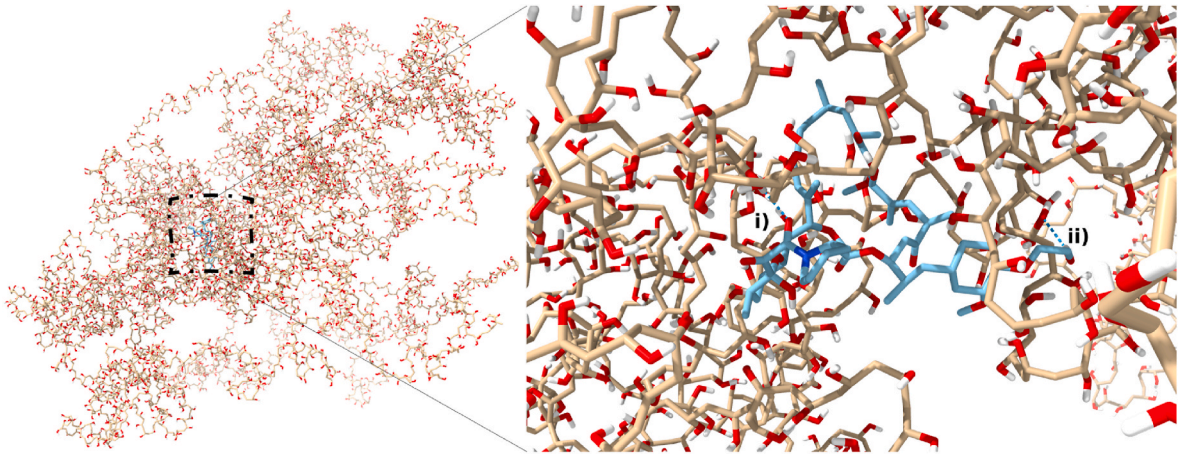

Fig. 4. Interaction between single EVR molecule with a polymer chain of PVA. The zoomed region shows the two-hydrogen bonding interaction, detailed in Fig. 5.

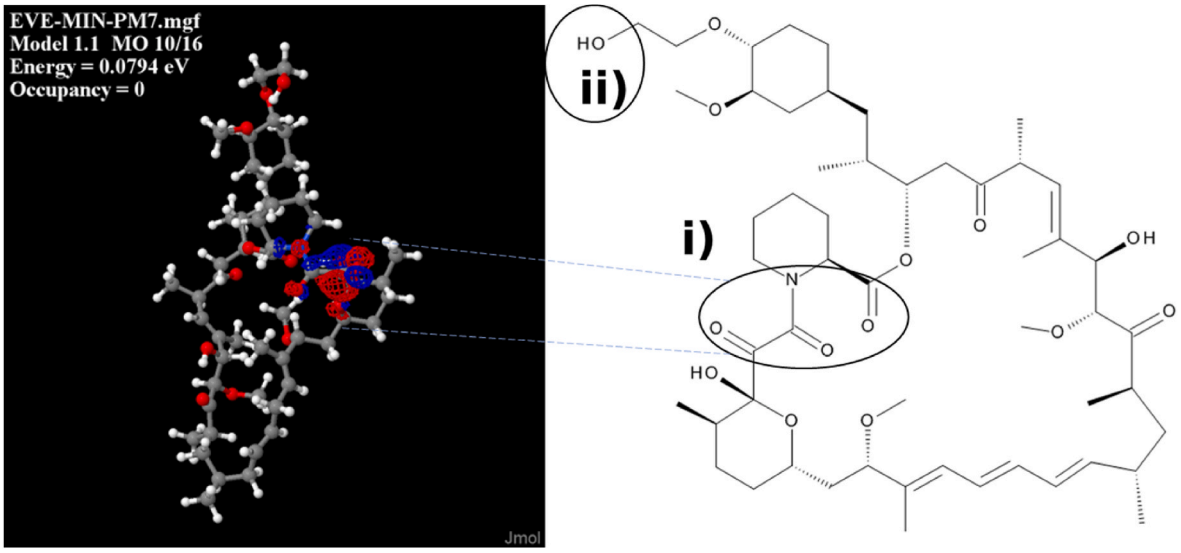

Fig. 5. Representation of the EVR molecule after parametric minimization following semi-empirical method and its 2D structure. The representation shows the hydrogen bonding interactions between PVA and EVR in i) shows the orbital lumo which was the region interacted with the PVA chain, whereas ii) is the hydrogen bond formed with a freer site of OH group.

suitable pre-defined geometries for drug delivery vehicles that allow for cell infiltration post gelation as well as better encapsulation of drug molecules post-crosslinking [39].

Although nanospheres are seen for the conjugated system PVA and EVR hydrogel, it is possible that a saturation occurred, albeit this limitation was not a drawback since from the images few nanospheres are observed [17].

3.4. *In vitro* EVR release study and weight loss studies

Following the development and characterisation of the PVA-EVR microspheres, the *in vitro* EVR release profile was evaluated to determine the duration taken for the PVA-EVR microspheres and solvent-cast PVA-EVR films to achieve a 50% EVR release. Fig. 7 show the average results of the *in vitro* EVR release from PVA-EVR microspheres and solvent-cast PVA-EVR films, respectively. Based on the results, the PVA-EVR microspheres steadily achieved 50% EVR release within 250–300 h before achieving up to 62.17% EVR release after 12.5 days. In contrast, solvent-cast PVA-EVR film only achieved 49.06% of EVR release and no further EVR release was observed after 4 h. The results confirmed that the PVA-EVR microspheres achieved a prolonged sustained release of EVR due to the crosslinking of the PVA and EVR during the freeze-thawing process as well as the encapsulation of EVR within the hydrophilic core of the PVA drug carrier. Therefore, the encapsulation resulted in the sustained release of EVR through the hydrophilic part of the PVA.

Table 3 shows the input of EVR release profile in various release kinetic models, including zero-order, first-order, Higuchi, Korsmeyer-Peppas, and Hixson-Crowell models. The Higuchi model provided the best fit ($R^2 = 0.9966$) kinetic modelling for the EVR release from the PVA-EVR microspheres, demonstrating that the EVR release seems to be a process predominately controlled by diffusion. The R^2 value for the Korsmeyer-peppas model was also high at 0.9893. According to the DDSolver software calculation for the Korsmeyer-Peppas model, the value of $n = 0.86$ characterises the release mechanism of the drug, suggesting a non-Fickian transport mechanism through microspheres [17]. Similarly, the Higuchi model provided the best fit ($R^2 = 0.9199$) for the EVR release from the solvent-cast PVA-EVR film, indicating that the EVR release via the diffusion-controlled release mechanism was comparable to that of PVA-EVR microspheres (Table 3). The EVR release pattern was also similar to the results reported in previous literature [17], indicating that the PVA-EVR microspheres provided a sustained release of EVR.

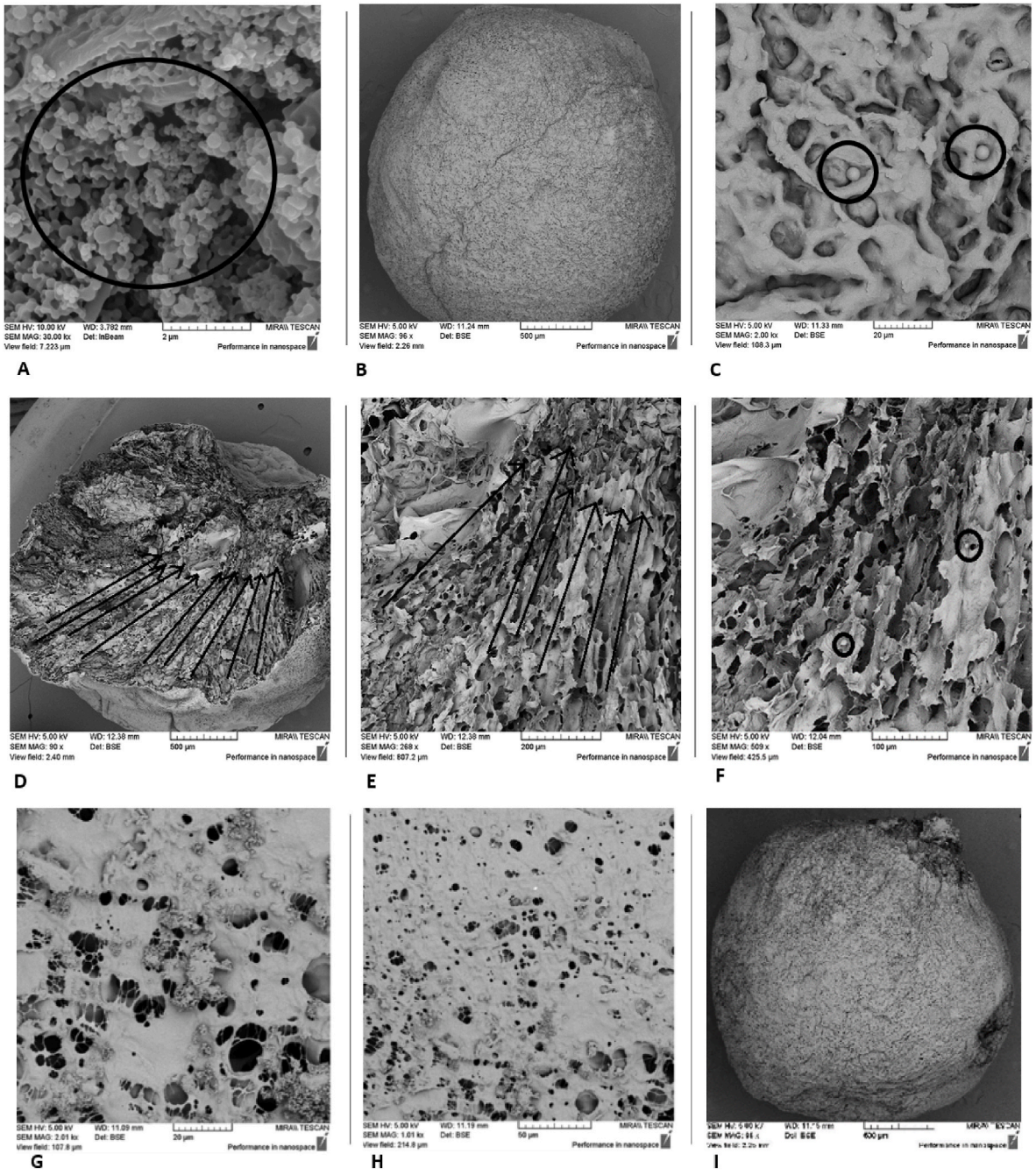

Fig. 6. SEM images of PVA microsphere and PVA-EVR microsphere (PVA concentration 5%wt.%, 195,000 g/mol, EVR 1 wt,%) a) Pure EVR powder (30 kX), b) Outer layer of PVA-EVR microspheres (96 X), c) Inner layer of PVA-EVR microspheres with embedded EVR spherical particles (2 X), d) Cross-sectional view of PVA-EVR microspheres (90 X), e) Uni-directional alignment of PVA-EVR microspheres (268 X), f) Cross-Sectional porous structure of the inner layer of PVA-EVR microsphere (1 kX), g) Porous structure of the inner layer of PVA-EVR microsphere (2 kX), h) Surface of PVA microsphere (500 X), and i) Outer layer of PVA microsphere (96 kX).

Additionally, the percentage weight loss was calculated post-*in vitro* dissolution studies using Equation (5). Based on the results, the percentage weight loss obtained for each PVA-EVR microsphere batch was 15%, 13.6%, and 16.56%, respectively. Therefore, the weight loss signifies the release of EVR from the microspheres. This result is supported by the EVR loading results.

3.5. Encapsulation efficiency (EE)

The EE evaluation and interpolation of the absorbance value were performed by plotting the calibration curve for this purpose ($y = 0.041x - 0.011$) (Supplementary Material Fig. S6). The obtained calibration curve was linear in the range of 0.0625–10 mg/mL with $R^2 = 0.9997$. According to Equation (2), the theoretical drug loading of EVR was 16.6%, while the actual drug loading and calculated EE from Equations (3) and (4) in the EVR-PVA microsphere were 18.29% and 76.67%, respectively. The encapsulation of hydrophobic EVR in the polymeric matrix of the microsphere promoted a remarkable EE. However, a 100% EE could not be achieved as some EVR may be lost during the initial stages of microsphere formation in pre-cooled ethanol the before the freeze-drying process.

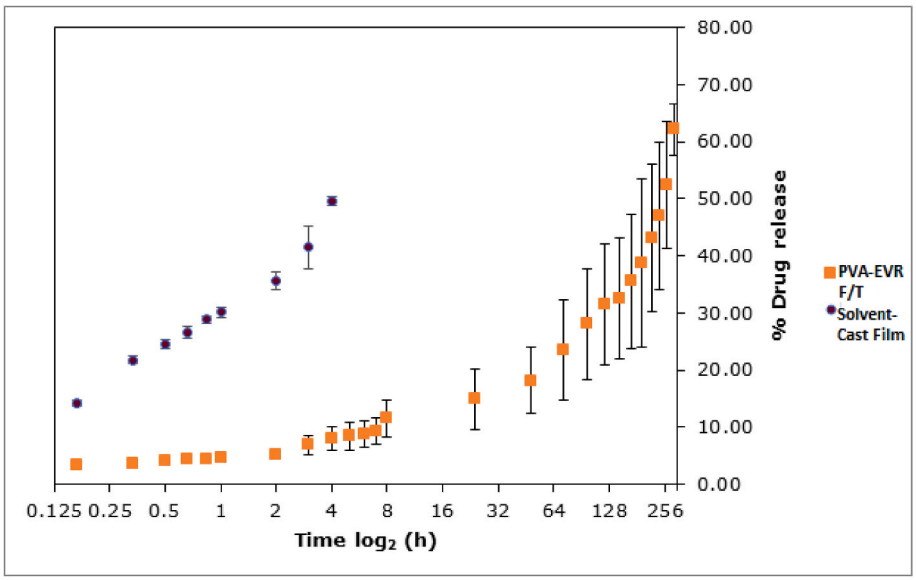

Fig. 7. Mean of the *In vitro* release of EVR from the PVA-EVR microspheres and EVR from the solvent-cast PVA-EVR film.

Table 3
Model fit parameters for the PVA-EVR microspheres within each kinetic model release.

F/T cycles	Zero order	First order	Higuchi	Korsmeyer-Peppas			Hixson–Crowell
	R^2	R^2	R^2	R^2	F_0	n	R^2
(6F/3T)	0.9577	0.5056	0.9966	0.9893	7.236	0.86	0.9414
Solvent-cast(no F/T)	0.7794	0.7415	0.9199	0.6927	6.342	0.371	0.8655

3.6. Swelling index and weight loss study

The swelling index was performed to measure the swelling degree of the PVA-EVR microsphere and PVA microsphere. This test was done in-triplicate. Fig. 8 depicts the degree of swelling as a function of time for PVA microsphere and PVA-EVR microspheres. In terms of water content, the PVA microsphere and PVA-EVR microspheres that underwent 6F/3T cycles reached an equilibrium swelling rate of 246.13% within 24 h of soaking in the buffer. This indicates that samples that were subjected to the freeze-thaw cycle required a shorter amount of time to reach an equilibrium swelling rate compared to those that were not subjected to the freeze-thaw cycle [17]. In contrast, PVA microspheres subjected to 6F cycles showed a maximum mean swelling ratio of 835.52% after 24 h of soaking.

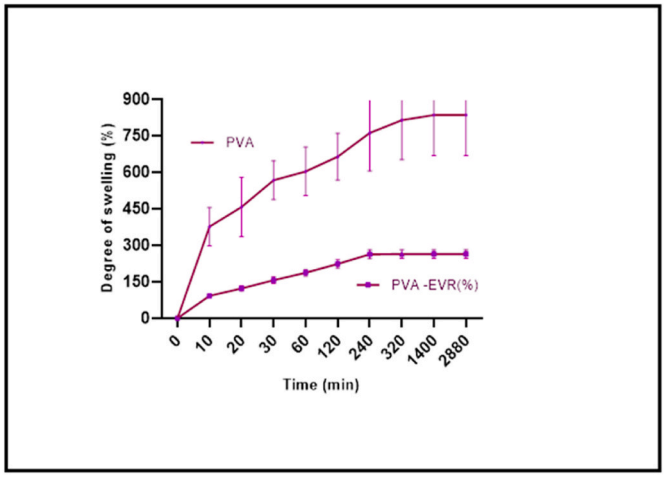

Fig. 8. Mean swelling degree of PVA microspheres samples and PVA-EVR microspheres.

The PVA microspheres and PVA-EVR microspheres samples are considered swelling-controlled release devices [35]. The EVR molecules are entrapped within the polymer matrix of PVA. When swelling occurs due to buffer absorption by the hydrogel, the molecular weight between crosslinks increases and caused the polymer to expand. Consequently, the drug diffusivity and release kinetics of the PVA-EVR was affected. Based on the observation, the PVA-EVR microspheres have a lower swelling degree than PVA microspheres, which may be attributed to an increase in mechanical properties of hydrogel, consequently, related to a better interaction between the drug and PVA as the chains cannot achieve a total relaxed state due to bound water and intermolecular bonds [45].

The SEM imaging also showed that the porosity of the microspheres increased the nutrient flux in the polymer matrix, which was influenced by the swelling of microspheres and its mechanical properties [46]. Furthermore, a normality test (Fig. 9) showed that the data were evenly distributed, while the one-way ANOVA test indicated a significant effect ($p < 0.005$) when the PVA microspheres were loaded with EVR. A significant difference in porosity of PVA-EVR ($p < 0.0001$) and PVA ($p < 0.05$) were also observed (see Figs. 6, 9 and 10).

3.7. X-ray diffraction analysis

The spectra profile from the studied samples exhibits a very broad profile indicating a more amorphous material. However, it is possible to see an increase in crystallinity by freeze-thawing. Nonetheless, the profile of pure drug also shows an amorphous profile with various peaks related to the various crystalline planes. Polyvinyl alcohol hydrogels present this typical broad profile, but samples with F/T crosslink distinctly presents the most defined peak from the EVR drug around 23° compared to solvent-cast films confirming the presence of the drug while

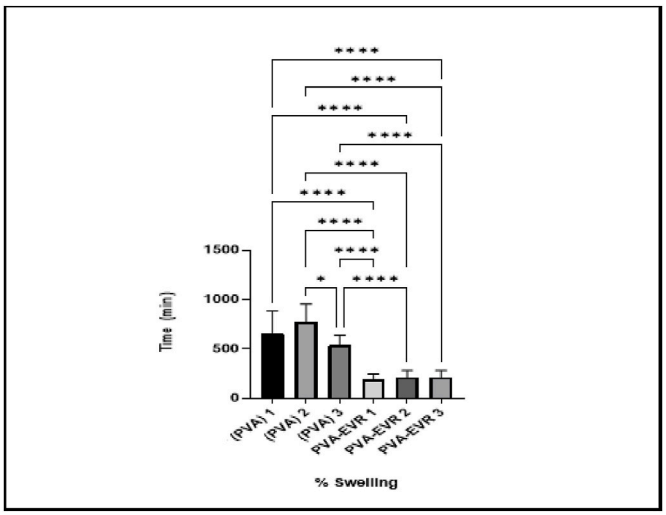

Fig. 9. Swelling index of PVA microspheres and PVA-EVR microspheres done in-triplicate. Data is shown only when there is a significant difference between the two samples. Statistical analysis was performed using the one-way ANOVA test, followed by the Tukey post-test. The level of significance is denoted by asterisks. $*p < 0.0105$ and $****p < 0.0001$.

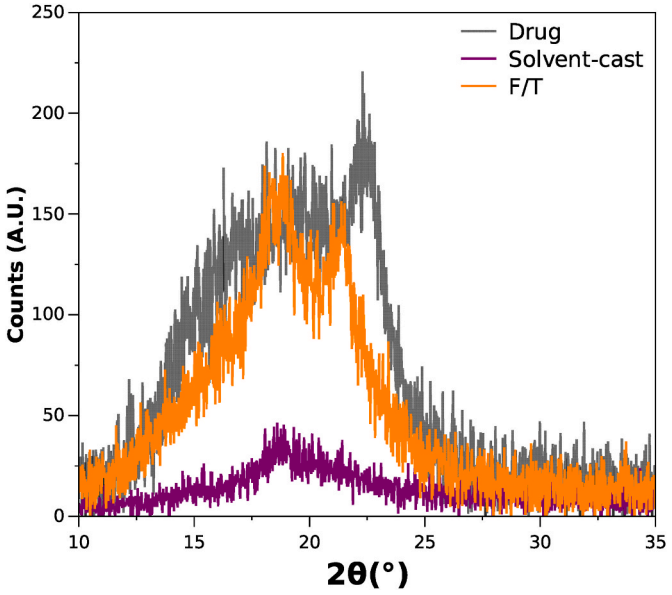

Fig. 10. X-ray diffraction analysis for pure drug, solvent cast films and freeze thawing hydrogels containing the drug.

also with a shift to lower angles which is expected based on FTIR analysis.

3.8. Docking of mTOR with everolimus

3.8.1. Docking simulation of mTOR protein with everolimus

Similarly, it is important to highlight the mechanism between EVR with the mTOR (mammalian target of rapamycin) protein. It is already reported by previous works that the inhibition of mTOR by rapamycin is dependent on formation of an interaction between binding protein FKBP which interacts with mTOR via hydrophobic rapamycin molecule that binds active sites. Due to the specific type of bonding, steric hindrance occurs and inhibits rapamycin. Therefore, interaction between FKBP and EVR is of the utmost importance. Docking interaction between both molecules (redocking with RMSD 0.45) presents that hydrogen bonding occurs for both FKBP and the mTOR with EVR, with three hydrogen bonds (Fig. 11). Docking interaction between both molecules (redocking with RMSD 0.45 – Supplementary Material Fig. S9) presents that hydrogen bonding occurs for both FKBP and the mtor with everolimus, with three hydrogen bonds. Moreover, the OH region at the terminus of the compound may present an improved interaction than its previous candidate drug (Sirolimus) with a binding energy of (−11.4 kcal/mol). Although associations of steric hindrance should be performed by molecular dynamics of both interactions, the system in question presents a good improvement compared to sirolimus and is a good candidate for the treatment of SEGA cells.

4. Conclusion

This study described the development of PVA-EVR microspheres for EVR delivery to treat SEGA-associated TSC disease. The optimised and stable PVA-EVR microspheres consisted of 5% w/v PVA Mowiol grade 56–98 and 1% w/v EVR and were subjected to the 6F/3T cycle. The SEM and FTIR characterisation proved the EE of EVR particles within the PVA matrix via weak chemical and physical interactions. In addition, the *in vitro* EVR release from the PVA-EVR microspheres recorded a sustained EVR release of 62.17% after 12.5 days compared to the EVR release of 49.06% after 4 days from the solvent-cast PVA-EVR films. The results showed that the PVA-EVR microsphere obeyed the Higuchi release model and confirmed that the PVA polymer enhanced the bioavailability of EVR. Therefore, PVA-EVR formulation with the sustained-release capability of EVR has the potential to serve as a prospective drug delivery system for the treatment of SEGA-associated TSC. The molecular docking study conducted, shows proper cross-linking was achieved between EVR and PVA from the repeated freezing and thawing cycles, which is further confirmed in the FTIR and XRD results.

The PVA based microspheres can be used as a locally implantable device post-surgical treatment to bypass systemic circulation compared to the current orally administered EVR treatment, reducing systemic toxicities associated with EVR This can also resolve solubility issues related with hydrophobic chemotherapeutic drugs. In conclusion, this study highlighted the advantages of PVA-EVR microspheres as a drug delivery system in treating SEGA associated TSC post-surgical resection.

Funding

Technological University of the Shannon, President Seed Fund.

CRediT authorship contribution statement

Lynn Louis: Methodology, Investigation, Validation, Formal analysis, Data curation, Writing – original draft, Writing – review & editing, Visualizsation. **Bor Shin Chee:** Methodology, Data curation, Writing – original draft, Writing – review & editing, Visualizsation. **Noreen Louis:** Investigation, Data curation. **Gabriel Goetten De Lima:** Methodology, Investigation, Data curation, Formal analysis, Software, Writing – review & editing. **Marion McAfee:** Investigation, Data curation. **Alan Murphy:** Data curation, Investigation. **Michael J.D. Nugent:** Conceptualizsation, Methodology, Supervision, Funding acquisition, Project administration, Resources.

Declaration of competing interests

The authors declare the following financial interests/personal relationships which may be considered as potential competing interests: Lynn Louis reports financial support was provided by Technological University of the Shannon Midlands Midwest - Athlone Campus. Lynn Louis reports a relationship with Technological University of the Shannon Midlands Midwest - Athlone Campus that includes: funding grants.

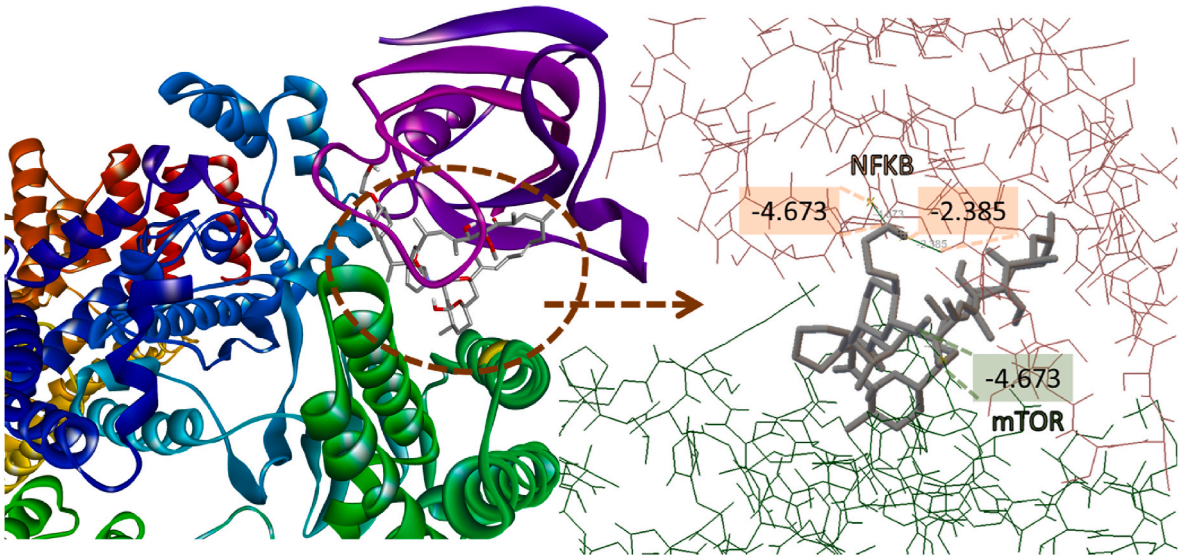

Fig. 11. Interaction of mTOR and NFKB with EVR; the detailed region, distinguished by the arrow, shows the hydrogen bonds, along with its binding affinity values, for the studied residual and subsequent protein.

Data availability

No data was used for the research described in the article.

Acknowledgements

This work was supported by the Technological University of the Shannon [President's Doctoral Scholarship].

Appendix A. Supplementary data

Supplementary data to this article can be found online at https://doi.org/10.1016/j.jddst.2023.104204.

References

[1] Y. Baron, A.J. Barkovich, MR Imaging of Tuberous Sclerosis in Neonates and Young Infants, 1999, p. 10.
[2] SEGA Tumors, Novartis, n.d. https://www.novartis.com/our-focus/cancer/oncology-disease-areas/sega-tumors. (Accessed 12 September 2021).
[3] M.S. Arroyo, D.A. Krueger, E. Broomall, C.B. Stevenson, D.N. Franz, Acute management of symptomatic subependymal giant cell astrocytoma with everolimus, Pediatr. Neurol. 72 (2017) 81–85, https://doi.org/10.1016/j.pediatrneurol.2017.04.008.
[4] D.N. Franz, E. Belousova, S. Sparagana, E.M. Bebin, M.D. Frost, R. Kuperman, O. Witt, M.H. Kohrman, J.R. Flamini, J.Y. Wu, P. Curatolo, P.J. de Vries, N. Berkowitz, J. Niolat, S. Jóźwiak, Long-term use of everolimus in patients with tuberous sclerosis complex: final results from the EXIST-1 study, PLoS One 11 (2016), e0158476, https://doi.org/10.1371/journal.pone.0158476.
[5] N. Mehra, Mohd Aqil, Y. Sultana, A grafted copolymer-based nanomicelles for topical ocular delivery of everolimus: formulation, characterization, ex-vivo permeation, in-vitro ocular toxicity, and stability study, Eur. J. Pharmaceut. Sci. 159 (2021), 105735, https://doi.org/10.1016/j.ejps.2021.105735.
[6] V. Beljanski, Everolimus, in: XPharm: the Comprehensive Pharmacology Reference, Elsevier, 2008, pp. 1–5, https://doi.org/10.1016/B978-008055232-3.64074-7.
[7] D. de Wit, T.C. Schneider, D.J.A.R. Moes, C.F.M. Roozen, J. den Hartigh, H. Gelderblom, H.J. Guchelaar, J.J. van der Hoeven, T.P. Links, E. Kapiteijn, N. P. van Erp, Everolimus pharmacokinetics and its exposure–toxicity relationship in patients with thyroid cancer, Cancer Chemother. Pharmacol. 78 (2016) 63–71, https://doi.org/10.1007/s00280-016-3050-6.
[8] B. Melendez, S. Shah, Y. Jiang, J. Dottino, E. Watson, H. Pearce, M. Borthwick, R. E. Schmandt, Q. Zhang, K. Cumpian, J. Celestino, B. Fellman, Y. Yuan, K.H. Lu, A. G. Mikos, M.S. Yates, Novel polymer-based system for intrauterine delivery of everolimus for anti-cancer applications, J. Contr. Release 339 (2021) 521–530, https://doi.org/10.1016/j.jconrel.2021.10.008.
[9] D.A. Krueger, M.M. Care, K. Holland, K. Agricola, C. Tudor, P. Mangeshkar, K. A. Wilson, A. Byars, T. Sahmoud, D.N. Franz, Everolimus for subependymal giant-cell astrocytomas in tuberous sclerosis, N. Engl. J. Med. 363 (2010) 1801–1811, https://doi.org/10.1056/NEJMoa1001671.
[10] C.J. Campen, B.E. Porter, Subependymal giant cell astrocytoma (SEGA) treatment update, Curr. Treat. Options Neurol. 13 (2011) 380–385, https://doi.org/10.1007/s11940-011-0123-z.
[11] P. Sun, M. Kohrman, J. Liu, A. Guo, J. Rogerio, D. Krueger, Outcomes of resecting subependymal giant cell astrocytoma (SEGA) among patients with SEGA-related tuberous sclerosis complex: a national claims database analysis, Curr. Med. Res. Opin. 28 (2012) 657–663, https://doi.org/10.1185/03007995.2012.658907.
[12] K. Giannikou, Z. Zhu, J. Kim, K.D. Winden, M.E. Tyburczy, D. Marron, J.S. Parker, Z. Hebert, A. Bongaarts, L. Taing, H.W. Long, W.V. Pisano, S. Alexandrescu, B. Godlewski, M. Nellist, K. Kotulska, S. Jozwiak, M. Roszkowski, M. Mandera, E. A. Thiele, H. Lidov, G. Getz, O. Devinsky, M.S. Lawrence, K.L. Ligon, D.W. Ellison, M. Sahin, E. Aronica, D.M. Meredith, D.J. Kwiatkowski, Subependymal giant cell astrocytomas are characterized by mTORC1 hyperactivation, a very low somatic mutation rate, and a unique gene expression profile, Mod. Pathol. 34 (2021) 264–279, https://doi.org/10.1038/s41379-020-00659-9.
[13] D.N. Franz, J. Leonard, C. Tudor, G. Chuck, M. Care, G. Sethuraman, A. Dinopoulos, G. Thomas, K.R. Crone, Rapamycin causes regression of astrocytomas in tuberous sclerosis complex, Ann. Neurol. 59 (2006) 490–498, https://doi.org/10.1002/ana.20784.
[14] P. Menei, C. Montero-Menei, M.-C. Venier, J.-P. Benoit, Drug delivery into the brain using poly(lactide-co-glycolide) microspheres, Expet Opin. Drug Deliv. 2 (2005) 363–376, https://doi.org/10.1517/17425247.2.2.363.
[15] X.-W. Han, H.-W. Zhang, H.-Y. Luo, X.-L. Zheng, Z. Yang, N. Hu, Y.-J. Liao, J. Yang, Preparation of poly(vinyl alcohol) microspheres based on droplet microfluidic technology, Chin. J. Anal. Chem. 46 (2018) 1269–1274, https://doi.org/10.1016/S1872-2040(18)61105-3.
[16] G.G. de Lima, B.S. Chee, V.F. Moritz, Y.J. Cortese, W.L.E. Magalhães, D.M. Devine, M.J.D. Nugent, The production of a novel poly(vinyl alcohol) hydrogel cryogenic spheres for immediate release using a droplet system, Biomed. Phys. Eng. Express. 5 (2019), 045017, https://doi.org/10.1088/2057-1976/ab2547.
[17] B.S. Chee, G. Goetten de Lima, D.M. Devine, M.J.D. Nugent, Investigation of the effects of orientation on freeze/thawed Polyvinyl alcohol hydrogel properties, Mater. Today Commun. 17 (2018) 82–93, https://doi.org/10.1016/j.mtcomm.2018.08.005.
[18] G.-M. Kim, P. Simon, J.-S. Kim, Electrospun PVA/HAp nanocomposite nanofibers: biomimetics of mineralized hard tissues at a lower level of complexity, Bioinspiration Biomimetics 3 (2008), 046003, https://doi.org/10.1088/1748-3182/3/4/046003.
[19] R. Ricciardi, F. Auriemma, C. Gaillet, C. De Rosa, F. Lauprêtre, Investigation of the crystallinity of freeze/thaw poly(vinyl alcohol) hydrogels by different techniques, Macromolecules 37 (2004) 9510–9516, https://doi.org/10.1021/ma048418v.
[20] G. Torres-Flores, A. Gonzalez-Horta, Y.I. Vega-Cantu, C. Rodriguez, A. Rodriguez-Garcia, Preparation and characterization of liposomal everolimus by thin-film hydration technique, Adv. Polym. Technol. 2020 (2020), e5462949, https://doi.org/10.1155/2020/5462949.
[21] Vamsikrishna Reddy, Drug release mechanism and kinetics, (18:11:34 UTC). https://www.slideshare.net/vamsikrishnareddy57/drug-release-mechanism-and-kinetics. (Accessed 31 July 2021).
[22] H.K. Shaikh, R.V. Kshirsagar, S.G. Patil, Mathematical models for drug release characterization: a review, World J. Pharm. Pharmaceut. Sci. 13 (2010) 123–133.
[23] R.K. Deshmukh, J.B. Naik, Aceclofenac microspheres: quality by design approach, Mater. Sci. Eng. C 36 (2014) 320–328, https://doi.org/10.1016/j.msec.2013.12.024.
[24] Z. Zhang, S.-S. Feng, The drug encapsulation efficiency, in vitro drug release, cellular uptake and cytotoxicity of paclitaxel-loaded poly(lactide)–tocopheryl

polyethylene glycol succinate nanoparticles, Biomaterials 27 (2006) 4025–4033, https://doi.org/10.1016/j.biomaterials.2006.03.006.
[25] B.S. Chee, G.G. de Lima, T.A.M. de Lima, V. Seba, C. Lemarquis, B.L. Pereira, M. Bandeira, Z. Cao, M. Nugent, Effect of thermal annealing on a bilayer polyvinyl alcohol/polyacrylic acid electrospun hydrogel nanofibres loaded with doxorubicin and clarithromycin for a synergism effect against osteosarcoma cells, Mater. Today Chem. 22 (2021), 100549, https://doi.org/10.1016/j.mtchem.2021.100549.
[26] M.D. Hanwell, D.E. Curtis, D.C. Lonie, T. Vandermeersch, E. Zurek, G.R. Hutchison, Avogadro: an advanced semantic chemical editor, visualization, and analysis platform, J. Cheminf. 4 (2012) 17, https://doi.org/10.1186/1758-2946-4-17.
[27] J.J.P. Stewart, Optimization of parameters for semiempirical methods VI: more modifications to the NDDO approximations and re-optimization of parameters, J. Mol. Model. 19 (2013) 1–32, https://doi.org/10.1007/s00894-012-1667-x.
[28] N.M. O'Boyle, M. Banck, C.A. James, C. Morley, T. Vandermeersch, G. R. Hutchison, Open Babel: an open chemical toolbox, J. Cheminf. 3 (2011) 33, https://doi.org/10.1186/1758-2946-3-33.
[29] Y.K. Choi, S.-J. Park, S. Park, S. Kim, N.R. Kern, J. Lee, W. Im, CHARMM-GUI polymer builder for modeling and simulation of synthetic polymers, J. Chem. Theor. Comput. 17 (2021) 2431–2443, https://doi.org/10.1021/acs.jctc.1c00169.
[30] N. Guex, M.C. Peitsch, SWISS-MODEL and the Swiss-Pdb Viewer: an environment for comparative protein modeling, Electrophoresis 18 (1997) 2714–2723, https://doi.org/10.1002/elps.1150181505.
[31] G.M. Morris, R. Huey, W. Lindstrom, M.F. Sanner, R.K. Belew, D.S. Goodsell, A. J. Olson, AutoDock4 and AutoDockTools4: automated docking with selective receptor flexibility, J. Comput. Chem. 30 (2009) 2785–2791, https://doi.org/10.1002/jcc.21256.
[32] O. Trott, A.J. Olson, AutoDock Vina, Improving the speed and accuracy of docking with a new scoring function, efficient optimization, and multithreading, J. Comput. Chem. (2009), https://doi.org/10.1002/jcc.21334. NA-NA.
[33] W. Pu, D. Fu, H. Xia, Z. Wang, Preparation of hollow polyurethane microspheres with tunable surface structures via electrospraying technology, RSC Adv. 7 (2017) 49828–49837, https://doi.org/10.1039/C7RA09831F.
[34] N.N. Costa, L. de Faria Lopes, D.F. Ferreira, E.M.L. de Prado, J.A. Severi, J. A. Resende, F. de Paula Careta, M.C.P. Ferreira, L.G. Carreira, S.O.L. de Souza, M.A. P. Cotrim, T. Boeing, S.F. de Andrade, R.L. Oréfice, J.C.O. Villanova, Polymeric films containing pomegranate peel extract based on PVA/starch/PAA blends for use as wound dressing: in vitro analysis and physicochemical evaluation, Mater. Sci. Eng. C 109 (2020), 110643, https://doi.org/10.1016/j.msec.2020.110643.
[35] M.J.D. Nugent, A. Hanley, P.T. Tomkins, C.L. Higginbotham, Investigation of a novel freeze-thaw process for the production of drug delivery hydrogels, J. Mater. Sci. Mater. Med. 16 (2005) 1149–1158, https://doi.org/10.1007/s10856-005-4722-7.
[36] M. Wu, L. Kleiner, F.-W. Tang, S. Hossainy, M.C. Davies, C.J. Roberts, Surface characterization of poly(lactic acid)/everolimus and poly(ethylene vinyl alcohol)/everolimus stents, Drug Deliv. 17 (2010) 376–384, https://doi.org/10.3109/10717541003762847.
[37] M.A.A. Maki, P.V. Kumar, S.-C. Cheah, Y. Siew Wei, M. Al-Nema, O. Bayazeid, A.B. B.A. Majeed, Molecular modeling- $_B$ ased delivery system enhances everolimus-induced apoptosis in caco-2 cells, ACS Omega 4 (2019) 8767–8777, https://doi.org/10.1021/acsomega.9b00109.
[38] S. Cao, X. Zhou, Y. Yang, W. Zhong, T. Sun, Selective substitution of 31/42–OH in rapamycin guided by an in situ IR technique, Molecules 19 (2014) 7770–7784, https://doi.org/10.3390/molecules19067770.
[39] D.S. Park, I.-H. Bae, M.H. Jeong, K.S. Lim, D.S. Sim, Y.J. Hong, S.-Y. Lee, E.J. Jang, J.-W. Shim, J.-K. Park, H.C. Lim, H.B. Kim, In vitro and in vivo evaluation of a novel polymer-free everolimus-eluting stent by nitrogen-doped titanium dioxide film deposition, Mater. Sci. Eng. C 91 (2018) 615–623, https://doi.org/10.1016/j.msec.2018.05.064.
[40] J.-Y. Shin, D.Y. Lee, J.I. Yoon, Y.-S. Song, Effect of CMC concentration on cell growth behavior of PVA/CMC hydrogel, Macromol. Res. 28 (2020) 813–819, https://doi.org/10.1007/s13233-020-8106-0.
[41] P. Tangthuam, J. Pimoei, A.A. Mohamad, F. Mahlendorf, A. Somwangthanaroj, S. Kheawhom, Carboxymethyl cellulose-based polyelectrolyte as cationic exchange membrane for zinc-iodine batteries, Heliyon 6 (2020), e05391, https://doi.org/10.1016/j.heliyon.2020.e05391.
[42] K. Dey, S. Ganguli, S. Ghoshal, M.A. Khan, R.A. Khan, Study of the effect of gamma irradiation on the mechanical properties of polyvinyl alcohol based gelatin blend film, OALib 1 (2014) 1–10, https://doi.org/10.4236/oalib.1100639.
[43] H.S. Mansur, C.M. Sadahira, A.N. Souza, A.A.P. Mansur, FTIR spectroscopy characterization of poly (vinyl alcohol) hydrogel with different hydrolysis degree and chemically crosslinked with glutaraldehyde, Mater. Sci. Eng. C 28 (2008) 539–548, https://doi.org/10.1016/j.msec.2007.10.088.
[44] M. Bahadoran, A. Shamloo, Y.D. Nokoorani, Development of a polyvinyl alcohol/sodium alginate hydrogel-based scaffold incorporating bFGF-encapsulated microspheres for accelerated wound healing, Sci. Rep. 10 (2020) 7342, https://doi.org/10.1038/s41598-020-64480-9.
[45] F.S. Matty, M.T. Sultan, A.K. Amine, Swelling Behavior of Cross-link PVA with Glutaraldehyde 28 (2015) 11.
[46] S.S. Silva, T.C. Santos, M.T. Cerqueira, A.P. Marques, L.L. Reys, T.H. Silva, S. G. Caridade, J.F. Mano, R.L. Reis, The use of ionic liquids in the processing of chitosan/silk hydrogels for biomedical applications, Green Chem. 14 (2012) 1463, https://doi.org/10.1039/c2gc16535j.